Sustainable Cities and Society 33 (2017) 27–44

Contents lists available at ScienceDirect

Sustainable Cities and Society

journal homepage: www.elsevier.com/locate/scs

# Microclimate and air quality investigation in historic hilly urban areas: Experimental and numerical investigation in central Italy

Veronica Lucia Castaldo[a], Anna Laura Pisello[a,b,*], Ilaria Pigliautile[a], Cristina Piselli[a], Franco Cotana[a,b]

[a] CIRIAF-Interuniversity Research Center, Engineering Department, Via G. Duranti 67, Perugia, Italy
[b] Department of Engineering, University of Perugia, Via G. Duranti 93, 06125 Perugia, Italy

ARTICLE INFO

*Keywords:*
Microclimate
Urban area
Continuous monitoring
Numerical analysis
Local boundary conditions
Outdoor thermal comfort
Air quality
Hilly historical city

ABSTRACT

Outdoor environmental comfort strongly affects the quality of life and depends on local microclimate phenomena. However, impact of local boundaries is still weakly studied in hilly urban historical layouts. Local microclimate variability and its influence on pedestrians' comfort in selected hilly historical urban areas with varying local boundaries in term of vegetation, surface materials, urban density, and air quality, is investigated. To this aim, a field monitoring is carried out during summer in hilly dense built environment and numerical analysis is performed. Monitoring campaigns show how higher density and surface roughness in the urban historical area reduce daily temperature fluctuation up to 3 °C, with higher night temperatures. Temperature discrepancies up to 5 °C are detected compared to suburban greener area. Moreover, inverse correlation between sky-view factor and nighttime cooling is registered, with mean temperature variation up to 6.6 °C. Numerical analysis shows different thermal comfort conditions within the same district, due to different local boundaries in terms of sky-view factor and surface materials properties. Maximum Predicted Mean Vote difference of 0.6 is detected in the same area. Findings demonstrate how impact of local boundaries needs to be accurately investigated, when analyzing quality of outdoor urban environment, to realistically predict citizens' outdoor thermal conditions.

## Introduction and research background

Nowadays, a huge research effort worldwide is being focused on the understating of local climate phenomena able to significantly affect the built environment in terms of outdoor thermal comfort and energy/environmental performance, from both a qualitative and a quantitative point of view. Moreover, the mutual relationship between urban environmental quality and citizens' contribution in affecting energy use and outdoor and indoor thermal comfort conditions has been largely investigated (Kim, 1992).

In particular, different approaches coupling experimental campaign, analytical modeling, and numerical analysis have been implemented over the course of the years in order to be able to accurately predict and assess local urban microclimate conditions and their variations (Mirzaei and Haghighat, 2010; Papanastasiou and Kittas, 2012; Morini, Touchaei, Castellani, Rossi, & Cotana, 2016; Mohsin and Gough, 2012; Busato, Lazzarin, & Noro, 2014). The impact of local phenomena such as Urban Heat Island (UHI) and heat waves (Oke, 1976) and their role in affecting citizens' quality of life in urban areas (Santamouris and Kolokotsa, 2015) have been studied within different climate zones (Bagiorgas and Mihalakakou, 2016; Lauwaet et al., 2016; Kolokotroni and Giridharan, 2008; Kolokotroni, Davies, Croxford, Bhuiyan, & Mavrogianni, 2010). Such local climate change phenomena (Luber and McGeehin, 2008; McMichael, Woodruff, & Hales, 2006a) are able to significantly affect the wellbeing and health of citizens in urban contexts, even exacerbated by energy poverty (Innovating to zero the building sector in Europe, 2016). In fact, they may have serious consequences at a local scale, e.g. in terms of outdoor thermal comfort for pedestrians (Rosso et al., 2015), human's health (McMichael, Woodruff, & Hales, 2006b), building energy consumption (Santamouris, 2014), and also from an economical point of view (Stern and Treasury, 2007).

Based on this background, microclimate variations of such urban/sub-urban environment and their impact on citizens' quality of life and buildings energy need are attracting increasingly interest from the scientific community. In fact, a deep understanding of the complex relationship existing between the built-environment and its microclimate can help to (i) reduce the negative effects of UHI phenomenon

* Corresponding author at: CIRIAF-Interuniversity Research Center, Engineering Department, Via G. Duranti 67, Perugia, Italy.
*E-mail addresses:* pisello@crbnet.it, anna.pisello@unipg.it (A.L. Pisello).

http://dx.doi.org/10.1016/j.scs.2017.05.017
Received 26 September 2016; Received in revised form 26 April 2017; Accepted 23 May 2017
Available online 29 May 2017

**Nomenclature**

| | |
|---|---|
| T | Air temperature [°C] |
| sT | Surface temperature [°C] |
| RH | Relative humidity [%] |
| $w_s$ | Wind speed [m/s] |
| ΔT | Temperature fluctuation [°C] |
| MRT | Mean Radiant Temperature [°C] |
| $X_{monitored}$ | Experimentally collected data |
| $X_{simulated}$ | Simulation output data |
| SVF | Sky-view factor |
| pt1, pt2 | Point 1 and point 2 of analysis of numerical simulation results |
| h | Horizontal |
| v | Vertical |
| rr | Reflected radiation [W/m$^2$] |
| lwr | Long-wave radiation [W/m$^2$] |
| $\mathbf{Q^{abs}_{sw,net}}$ | Absorbed incoming short wave radiation [W] |
| $\mathbf{Q^{abs}_{lw,net}}$ | Absorbed incoming long wave radiation [W] |
| ε | Emissivity [%] |
| σ | Stefan-Boltzman constant |
| $\mathbf{h_{c,o}}$ | Convection coefficient for the i-th outside wall [W/m$^2$·K] |
| λ | Heat transfer coefficient [W/m·K] |
| $\Delta x$ | Distance between two nodes [m] |
| $\mathbf{c_{wall}}$ | Heat capacity of the wall [J/kg·K] |
| $\mathbf{T_n}$, $\mathbf{T^*_n}$ | Temperature at node n at present or future time step [°C] |
| $I_{cl}$ | Clothing insulation [clo] |
| UHI | Urban heat island |
| UH | Urban historical area |
| UR | Urban recent area |
| SG | Suburban green area |
| SB | Suburban built area |
| MBE | Mean bias error |
| RMSE | Root mean square error |
| TMY | Typical meteorological year |

and heat waves events, (ii) find suitable mitigation strategies for each specific urban context, and (iii) support an environmentally sustainable and energy efficient urban planning.

In this view, Santamouris, Cartalis, and Synnefa (2015) showed how the awareness about risky microclimate conditions in a city could help to develop the most appropriate resilience plan for allowing citizens to face Urban Heat Island effects. Specific policy issues and tailored mitigation measures were proposed for the city of Athens (Greece) to quantify the magnitude and the spatial variation of UHI and its implications on building energy consumption and pedestrians' comfort. A similar approach including numerical analysis was adopted by Galli, Vallati, Recchiuti, de Lieto Vollaro, and Botta (2013), who developed a 3D model of a district in Rome (Italy). The percentage of greenery was gradually increased to study effects in local microclimate variation. Similarly, Taleghani, Kleerekoper, Tenpierik, and van den Dobbelsteen (2014) simulated the relationship between the urban environment configuration and its microclimate by elaborating models of five idealized simple urban layouts. The aim was to provide basic suggestions for urban planners which could be easily adapted to realistic situations. Alvarez (2001) investigated the reason why the ancient neighborhood of Santa Cruz (Spain) presents better thermal behavior during summer compared to new areas of the city, where an UHI effect of 2–3 °C was detected, in particular during night. The simulation of the old city area showed that peculiar characteristics, such as the presence of trees and water fountains, walls high thermal mass, streets aspect ratio and orientation, can significantly improve the environment thermal behavior during extreme conditions.

At local scale, the alteration of microclimate parameters in urban areas is mainly due to a modification of the energy balance. Such modification is due to several factors, e.g. substitution of green areas with impermeable surfaces, limited evapotranspiration, poor thermal/physical properties of construction surfaces often characterized by low albedo, geometry of the urban settlement in terms of orientation and aspect ratio, presence of anthropogenic heat sources (i.e. factories, traffic, or HVAC systems) (Giridharan, Lau, Ganesan, & Givoni, 2007; Taha, 1997). The impact of peculiar boundary conditions on the urban microclimate and thermal comfort at local scale has been largely investigated by the scientific community. The influence of urban geometry on both heat fluxes and pedestrians' thermal comfort was investigated for a canyon in three Moroccan climatic zones by Jihad and Tahiri (2016). Different aspect ratios were calculated to ensure acceptable Predicted Mean Vote (PMV) levels in each zone. Similarly, Consuegra and Matzarakis (2016) evaluated the effects on Physiological Equivalent Temperature (PET) of street orientation and aspect ratio. The impact of built-up surfaces on land surface temperatures was also investigated in (Morabito et al., 2016) for selected Italian urban areas. Daytime and nighttime land surface temperature slope patterns were detected to be dependent on city size and urban morphology. In the hot-humid climate of Colombo (Sri Lanka) (Emmanuel, 2005), an increasing trend of thermal discomfort, mainly during night, was registered in the suburban station. This phenomenon was found to be correlated with hard land cover modifications. In the same scenario, Georgakis, Zoras, and Santamouris (2014) simulated through a validated CFD model the application of cool covers on pavement and walls inside a canyon. Surface temperature reduction up to 7–8 °C at ground level and 2–3 °C on walls, and air temperature decrease of about 1 °C were detected.

Despite the huge variability of ancient urban contexts and climate conditions, only a few of several existing microclimate studies are focused on the analysis of historic city districts. For instance, Noro, Busato, and Lazzarin (2015) investigated the UHI of the old city area of Padua (Italy). Results indicated the presence of UHI effect in urban zones up to 6 °C of air temperature increase. With the same aim, the local microclimate of the Malaysian historic town of Malacca was analyzed in (Jamei and Ossen, 2012). The heritage core zone was detected to be threatened by extremely high temperatures.

Within this research context, the present work investigates the relation between the local urban configuration and its microclimate in a historical city. The study was performed by means of both experimental and numerical approach, by paying particular attention on the characterization of microclimate conditions in the case study historical urban area. Therefore, a detailed and replicable methodology to evaluate the local microclimate conditions in such historic urban neighborhood, characterized by high architectural and cultural value, is here proposed. Moreover, the impact on humans' outdoor comfort conditions is highlighted.

## Motivation

Building upon the presented background, this work analyses the impact of boundary conditions, in terms of spatial-architectural configuration of the surrounding built environment, on local microclimate in urban contexts. In particular, the study is focused on the outdoor thermal comfort conditions for pedestrians in historical districts. In fact, buildings density and typology, in addition to vegetation, surfaces finishing, and anthropogenic actions, can significantly affect citizens' quality of life, especially in ancient urban areas. Therefore, an integrated methodology coupling experimental analysis and numerical modeling is proposed. The aim is to evaluate the outdoor environmental quality of the urban environment, i.e. thermal comfort and air quality

(Grimmond, King, Cropley, Nowak, & Souch, 2002; Cheung, Schiavon, Gall, Jin, & Nazaroff, 2017), by taking into account the impact of local boundary conditions and constrains of the surrounding context. More in detail, the purpose and the novelty of the research are as follows:

i to investigate and quantify the variability of the local microclimate of urban areas situated in the same city but characterized by different local boundaries in terms of density, vegetation, surface materials, and anthropogenic activities;
ii in particular, to determine the local environmental conditions and air quality of typical historic districts, where high construction density and low sky-view factor (SVF) affect pedestrians' thermal perception, but less pollution or anthropogenic heat is detected compared to new urban developments;
iii to analyze pedestrians' outdoor thermal comfort conditions eithin the historical urban area, i.e. the area characterized by the worst local microclimate conditions due to night overheating phenomena generated by the high density, low sky-view factor, and massive historical architectures.

In this view, the present study aims at filling the gap in UHI research where mainly historical and new flat urban areas are investigated, while ancient urban districts, typically situated on top of sloping hills for historical military protection purposes, have not been studied in detail. Nevertheless, they represent more than a half of the whole construction stock in Mediterranean countries.

The proposed approach consists of (i) the experimental continuous monitoring of microclimate variations in four selected urban and suburban areas characterized by different local constrains, and (ii) the detailed numerical analysis of the local microclimate in the historic urban neighborhood.

Four different urban contexts, i.e. an urban historic area, a recently developed neighborhood, a suburban built area, and a suburban vegetated area, were selected in the same city, therefore, within the same temperate climate zone. The case study city is Perugia, a middle-size city in central Italy characterized by a variable urban pattern and a deep historic urban layout (Fig. 1). The old city core was born with the first Etruscan settlement around the second half of the VI century b.C. Therefore, after 295 b.C. the Roman domination strongly influenced the development and expansion of the city by following the typical roman architectural style, yet preserving the original ancient Etruscan city center and narrow streets layout.

A preliminary monitoring campaign, carried out during summer, allowed to collect the main microclimate parameters within the four different case study areas in order to investigate the relation between local microclimate and urban air quality. Afterwards, a numerical analysis was performed in order to predict and analyze the local microclimate distribution in the historical urban area.

The innovative purpose is to highlight (i) the local microclimate differences occurring in different areas situated within the same climate zone and (ii) the correlation between such microclimate variation and specific local boundary conditions, which have a non-negligible role in affecting the environmental quality of the urban environment. Moreover, the present comprehensive study aims at analyzing specifically the impact of the detected local microclimate variations on pedestrians' outdoor thermal comfort in the context of the historic area of


**Fig. 1.** Views of the historical center of Perugia: (a) the main street, Corso Vannucci, (b) Porta Sole (top of the ancient hill) in the North, (c) the main square, Piazza IV Novembre.

the city, characterized by irregular urban layout and architectural configuration typically generating a discomfortable thermal environment.

## 3. Methodology

The research methodology included two main steps, namely (i) a preliminary experimental monitoring campaign and (ii) the numerical modeling of the urban historic case study area. During the first phase, the main outdoor microclimate parameters were collected under the same meteorological conditions in the four urban areas, which were specifically selected for their varying construction density, building materials, construction period, and amount of outdoor greenery.

After the post-processing of the collected microclimate data, the numerical analysis was performed to evaluate pedestrians' outdoor thermal comfort within the historic neighborhood in both summer and winter conditions.

The main steps of the research study are summarized in Fig. 2.

### 3.1. Experimental monitoring campaign

The city of Perugia, in central Italy (43°6′44″N, 12°23′20″E), is classified as Cfa (i.e. humid subtropical climate) in the Köppen-Geiger climate classification (Köppen-Geiger, 2017 *Köppen-Geiger climate classification updated using temperature and precipitation data referring to the period 1951–2000*). Therefore, it is characterized by hottest months with average temperatures above 22 °C and high precipitation level. Under these general conditions, microclimate parameters can change at microscale level, i.e. within the urban canopy layer, due to the strong impact of the local boundaries.

In order to understand the impact of such local phenomena and analyze the microclimate spatial variation due to different boundary conditions at urban scale, a monitoring campaign was carried out during summer in different areas of the city. In fact, such medium-size city presents a well-defined and compact historic center, modern suburbs, and suburban-rural residential areas.

With the aim of characterizing the local microclimate spatial variation, three different locations representative of the three above mentioned typical urban configurations were selected. Additionally, a fourth case study area, representative of the suburban building area, was selected as reference case scenario. In this area, the weather data were continuously collected for the whole monitoring period.

The four case study areas are briefly described below, also referring to the Local Climate Zone (LCZ) classification provided by Stewart and Oke (Stewart and Oke, 2012). Moreover, their location within the city of Perugia is shown in Fig. 3.

*Urban Historical area (**UH area**):* it is the dense historical city center neighborhood, mid-rise local climate zone according to LCZ classification. Buildings are generally characterized by thick stone walls and outdoor pavements are covered by bricks and slabs mainly made of *pietra serena*, typical of the historic area. The monitoring station was positioned in an East-West oriented street at about 15 m from the ground, facing South.

*Urban Recent area (**UR area**):* it is a partially traffic-congested area connecting the area hosting the city main train station to the city center, and it can be considered as open mid-rise zone according to LCZ. Buildings are characterized by reinforced concrete structure and brick walls. The monitoring station was positioned at about 15 m from the ground, facing South.

*Suburban Green area (**SG area**):* it is a suburban residential area characterized by very low construction density and high presence of greenery, i.e. a sparsely built LCZ. Buildings are single-family houses with no more than two levels. A weather station is permanently located over the roof of one of these houses, inside a private green area at about 15 m from the ground, in open field.

*Suburban Built area (**SB area**):* it is another suburban area characterized by an intermediate built density between SG and UR and, referring to LCZ classification, it can be assimilated to open mid-rise zone. This position corresponds to the University campus of Perugia, selected as the reference case study. It consists of two large asphalted parking areas and seven blocks of buildings, located at different levels, with a concrete structural system and brick walls. A weather station is permanently located above the roof of the building situated in the highest part of the campus. Therefore, the collected data are assumed to be not affected by the presence of buildings in close proximity that is the reason why it was selected as reference case for this study.

In the last two case study areas, i.e. SG and SB, two continuously monitoring weather stations have been operating since 2010 and 2012, respectively. These stations register every 10 min the mean, minimum, maximum, and standard deviation value of the following weather parameters: dry-bulb temperature [°C], relative humidity [%], global solar radiation [W/m$^2$], wind speed [m/s] and direction [°], and rainfall rate [mm]. Such parameters are collected by the sensors every 20 s (and 5 s for those ones related to wind measurements) (Pisello, 2015).

In the other two case study areas, i.e. UH and UR, a portable monitoring station based on a Wireless Sensor Network system was used. It is composed of (i) sensors, (ii) collecting nodes, (iii) a data gathering gateway, and a dedicated (iv) software. The monitoring setup includes roughly the same kind of sensors described for the previously mentioned permanent stations, apart from the rain gauge. Sensors are directly connected via cable to nodes, which send the received signal via wireless to the gateway, able to store all the data by means of the on-board memory. Additionally, surface temperature probes and a carbon dioxide concentration sensor are provided with the purpose to combine the analysis of the urban thermal environment with the evaluation of air quality. In fact, wind speed within dense cities is usually lower due to presence of buildings. Therefore, the air mass transportation, including greenhouse gases, is strongly affected by the activation of convective cells. The main sensors characteristics are summarized in Table 1.

The monitoring campaign was carried out during June-July 2015. The data collected in the suburban green area, i.e. SG, and in the

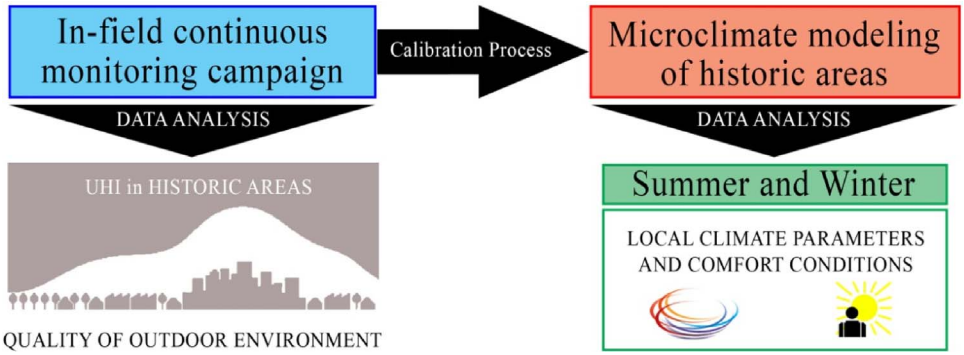


**Fig. 2.** Scheme of the methodology implemented in this research.

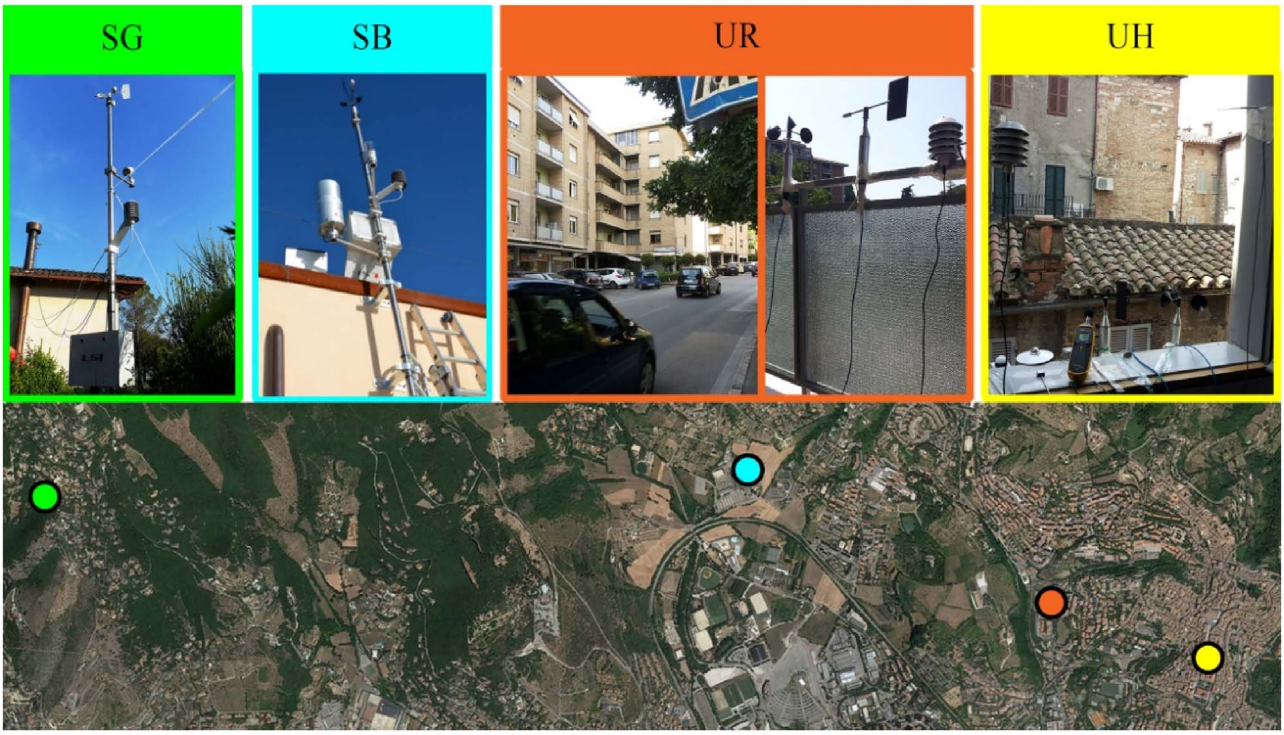


**Fig. 3.** Location of the four case study within the city of Perugia and pictures of the weather stations respectively installed.

reference case study area, i.e. SB, cover the whole two-month period since permanent weather stations were used. On the contrary, separate monitoring campaigns were carried out for the other two case study areas, i.e. UR and UH, since the same portable station was used for both of them. Therefore, for these last two areas data from the longest monitored period with consistent outdoor boundary conditions, i.e. clear sky and equivalent short-wave solar radiation, in terms of trend and intensity, were selected for the comparative analysis:

- June, 9th-12th for UR area;
- June, 30th- July, 2nd for UH area.

### 3.2. Elaboration and calibration of the model

A realistic model of the UH area (Fig. 4) was elaborated and calibrated by using the data collected during the first part of the study. The process of calibration and validation of the model was performed according to the ASHRAE Guideline 14 (ANSI/ASHRAE, 2002), by means of experimental data collected by two hygrothermal sensors. Such probes were positioned in two different points of the area, i.e. point A and point B, at 2 m height from the ground (Fig. 4d).

To numerically assess the correlation between (i) local microclimate and (ii) specific constrains of the area, the 3D model (Fig. 4e) was developed in order to include the monitored street and the two main cross streets. Therefore, the model comprehends all the surfaces materials characterizing the selected urban environment, i.e. buildings stone walls, historical stone pavement, and the asphalted recently repaved area, located in the West side of the street. Moreover, the dimensions of the 3D unit of the grid were set equal to 1 m in the x-y plane and to 2 m in height, in order to provide high spatial resolution and consider the necessary street slope discretization. Finally, a geometrical rotation of the model of 111° North out of the grid was imposed. Therefore, the model of the area is based on a 30 × 60 horizontal grid which grows 35 cells in height.

Given the impossibility to carry out invasive experimental analyses to characterize the construction materials properties, buildings

**Table 1**
Technical details of the sensors and monitored parameters.

| Sensors | Monitored Parameters | Measurement features |
|---|---|---|
| Wind speed anemometer (cup) | Wind speed [m/s] | Accuracy: < 0.1 m/s |
| Wind direction anemometer (flag) | Wind direction [°] | Resolution: 0.1°<br>Accuracy: 1° |
| Thermo-hygrometer | Air temperature [°C]<br>and Relative Humidity [%] | Accuracy: ± 0.3 °C<br>and ± 2.5% |
| Surface Temperature probes* | Surface Temperature [°C] | Accuracy: < 0.1 °C |
| Pyranometer | Incoming global solar radiation [W/m$^2$] | Sensitivity: 10 μV/(kW m$^2$)<br>Measure range: 0–2000 W/m$^2$ |
| $CO_2$ Transmitter | $CO_2$ concentration [ppm] | Measure range: 0–2000 ppm<br>Accuracy: < ± 50 ppm +2% of measured value |
| Rain gauge | Rainfall rate [mm] | Accuracy: 0 ÷ 1 mm/min: 1%;<br>1 ÷ 3 mm/min: 2%; 3 ÷ 5 mm/min: 4%;<br>5 ÷ 10 mm/min: 8% |

* two surfaces for each case study area were selected (one vertical and one horizontal), all with different materials.
- UR area: horizontal surface: marble, vertical surface: brick.
- UH area: horizontal surface: wood, vertical surface: “travertino”.


**Fig. 4.** Views of the UH area, from the (a) western and (b, c) eastern side; (d) position of the hygrothermal sensors used for the calibration of the model and (e) view of the 3D corresponding model.

envelope package and soil profiles were defined from the software database based on (i) preliminary field surveys (Pisello, Piselli, & Cotana, 2015), (ii) similar experimental analyses performed by the same authors in a previous work concerning traditional constructions (Bianchi, Pisello, Baldinelli, & Asdrubali, 2014), and (iii) characteristics of the surrounding buildings materials in the selected case study area (Pisello, Castaldo, Pignatta, Cotana, & Santamouris, 2016). The thermo-physical properties of materials used as input data for microclimate simulations are summarized in Table 2.

The data measured in the UH area by the microclimate station located at 15 m and by the two hygrothermal sensors positioned 2 m above the ground were used as input data for the model validation process. More in detail, the following parameters were considered:

- initial wind speed: value collected from the weather station at 6:00 a.m., which is the start-time of the simulation;
- wind direction: prevailing value during the three days monitoring campaign;
- 24 h air temperature and relative humidity forcing: data collected by the southern hygrothermal probe (Fig. 4d, point B).

In order to assess the reliability of the model, the gap between the simulation output data and the experimental measurements was analyzed in terms of air temperature and relative humidity. The calibration was carried out by comparing data collected by the northern hygrothermal sensor (Fig. 4d, point A) and those ones extracted in the corresponding point of the model. Moreover, the following calibration indexes are evaluated to test the accuracy of the numerical model (Salata, Golasi, De Lieto Vollaro, & De Lieto Vollaro, 2016a):

1- *Mean Bias Error* (Eq. (1)):

$$MBE = \frac{1}{n}\sum \left(x_{simulated} - x_{monitored}\right) \quad (1)$$

2- *Root Mean Square Error* (Eq. (2)):

$$RMSE = \sqrt{\frac{1}{n}\sum \left(x_{simulated} - x_{monitored}\right)^2} \quad (2)$$

- Willmott's index of agreement (Eq. (3)):

$$d = 1 - \frac{\sum_{i=1}^{n} |X_{simulated} - X_{monitored}|}{\sum_{i=1}^{n} \left(|X_{simulated} - \overline{X_{monitored}}| + |X_{monitored} - \overline{X_{monitored}}|\right)} \quad (3)$$

By considering (i) that simulations have to run for at least 6 h to get reliable results according to software developers' suggestions (ENVI-met software, 2017) and (ii) the dimensions of the model, the total run time simulation was set to 24 h.

### 3.3. Numerical analysis

This section provides technical details about the simulation tool used for the numerical analysis, in terms of numerical discretization scheme and physical equations implemented.

A three-dimensional microclimate modeling software, i.e. ENVI-met V4 (ENVI-met software, 2017; Huttner, Bruse, & Dostal, 2009), was selected mainly for its high accuracy in space, which allowed to study urban microclimate variation within the urban canopy layer (Terjung and O'Rouke, 1980). More in detail, the ENVI-met modeling environment uses the orthogonal Arakawa C-grid as numerical discretization scheme. Therefore, topography is included by creating cells filled with soil. Moreover, both the exposition and inclination of ground surfaces are considered for the energy balance calculations. The 3D CFD model of the wind field is based on the Reynolds-averaged non-hydrostatic Navier-Stokes equations (RANS), solved for each grid in space and each time step. Turbulence in the air is taken into account thanks to the Turbulence Kinetic Energy (TKE) model describing the distribution of kinetic energy and its dissipation rate. Moreover, the software models the fluxes of short and long-wave radiation and determines air temperature and humidity based on the calculated 3D wind field and the existence of sources or sinks of sensible heat and vapor. The heat in-

**Table 2**
Thermo-physical properties of the materials in the historic case study area.

| Element | | Property | Value |
|---|---|---|---|
| Walls | | Albedo | 0.3 |
| | | Emissivity | 0.9 |
| | | Specific heat | 840 [J/kg K] |
| | | Thermal conductivity | 0.86 [W/m K] |
| | | Density | 930 [kg/m$^3$] |
| Roofs | | Albedo | 0.5 |
| | | Emissivity | 0.9 |
| | | Specific heat | 800 [J/kg K] |
| | | Thermal conductivity | 0.84 [W/m K] |
| | | Density | 1900 [kg/m$^3$] |
| Profiles | Brick Road | Albedo | 0.3 |
| | | Emissivity | 0.9 |
| | | Volumetric Heat Capacity of the upper soil | $2{\cdot}10^6$ [J/m$^3$ K] |
| | | Heat Conductivity of the upper soil | 1 [W/m K] |
| | Basalt Brick Road | Albedo | 0.8 |
| | | Emissivity | 0.9 |
| | | Volumetric Heat Capacity of the upper soil | $2.39{\cdot}10^6$ [J/m$^3$ K] |
| | | Heat Conductivity of the upper soil | 1.73 [W/m K] |
| | Asphalt Road | Albedo | 0.2 |
| | | Emissivity | 0.9 |
| | | Volumetric Heat Capacity of the upper soil | $2.25{\cdot}10^6$ [J/m$^3$ K] |
| | | Heat Conductivity of the upper soil | 0.9 [W/m K] |

terchanged by built surfaces with atmosphere is also considered. The thermo-physical properties of building components considered in calculations are thickness, solar reflectance, thermal emissivity, absorption capability, transmission capability, heat transfer coefficient, and heat capacity. Therefore, the calculation of façades surface temperature is based on a 3-node transient state model. The finite difference method is used to solve partial differential equations in the model.

The energy balance of outer façades surface can, therefore, be written as follows (Eq. (4)):

$$Q_{sw,net}^{abs} + Q_{lw,net}^{abs} - \varepsilon\sigma T_{1,2}^4 + h_{c,o}(T_{air} - T_1^*) + \frac{\lambda}{\Delta x}(T_2^* - T_1^*) = \frac{c_{wall}\rho\Delta x}{2\Delta t}(T_n^* - T_n) \quad (4)$$

where:

- $Q_{sw,net}^{abs}$ is the absorbed incoming short-wave radiation [W];
- $Q_{lw,net}^{abs}$ is the absorbed incoming long-wave radiation [W];
- ε is the emissivity [%];
- σ is the Stefan-Boltzman constant;
- is the convection coefficient for the i-th outside wall [W/m$^2$ K];
- λ is the heat transfer coefficient [W/m K];
- Δ$x$ is the distance between two nodes [m];
- is the heat capacity of the wall [J/kg K];
- and$T_n^*$ are temperatures at node n at present or future time step, respectively.

By considering the Fourier Equation (Eq. (5)):

$$\frac{\delta T}{\delta t} = \frac{\lambda}{c_{wall}\rho}\frac{\delta^2 T}{\delta x^2} \quad (5)$$

the energy fluxes at the node in the center of the i-th wall are written as follows (Eq. (6)):

$$(P + 2)T_2^* - T_3^* = PT_2 + T_1^* \quad (6)$$

where $P$ is defined as follows (Eq. (7)):

$$P = \frac{\Delta x^2 c_{wall}\rho}{\lambda\Delta t} \quad (7)$$

Therefore, the energy balance for the node inside the wall becomes (Eq. (8)):

$$-T_2^* + \left(\frac{P}{2} + \frac{h_c\Delta x}{\lambda} + 1\right)T_3^* = \frac{P}{2}T_3 + \frac{h_{c,i}\Delta x}{\lambda}T_i \quad (8)$$

where hc,i is the heat convection coefficient inside the wall, i.e. 7.7 W/m$^2$ K.

The microclimate simulation of the monitored historical urban area (UH area) was performed in order to investigate (i) its environmental parameters and (ii) the pedestrians' comfort level, both in summer and winter conditions. To evaluate the outdoor thermal comfort conditions, a comparison in terms of PMV values (Yang, Zhao, Bruse, & Meng, 2013), provided by ENVI-met, PET index (Chirag and Ramachandraiah, 2010), calculated by means of RayMan software (Matzarakis, Rutz, & Mayer, 2007), and MOCI index (Mediterranean Outdoor Comfort Index) (Salata, Golasi, de Lieto Vollaro, & de Lieto Vollaro, 2016b) was carried out. A detailed presentation of the three indexes is provided in the following section.

### 3.4. Thermal comfort indexes

To evaluate the outdoor thermal comfort within the modeled area, three different indexes were calculated and compared.

The PMV index is based on the Fanger comfort model (Yang et al., 2013), which was initially developed to assess human thermal comfort in steady-state indoor conditions. Afterwards, it was adapted to outdoor environments by extending parts of the model related to energy fluxes with solar and long-wave radiation and taking into account higher wind speeds, suitable for outdoor applications. Despite these changes, the PMV is a stationary value and, therefore, it assumes that people are exposed for a sufficient time period to constant climate conditions. For this reason, other indexes, such as PET and MOCI, were calculated, since they are considered to be more representative of outdoor perceptions compared to PMV.

The PET index, as suggested by the German guidelines in urban and regional planning (Association of German Engineers, 1998), is based on the Munich Energy-balance Model for Individuals (MEMI) (Hoppe, 1999) and is defined as the air temperature in a standardized indoor setting at which the heat balance of the human body is balanced at the same core and skin temperature as under the outdoor conditions being assessed. On the other hand, the MOCI index is a novel thermal index elaborated specifically for the assessment of Mediterranean outdoor areas. It is based on the ASHRAE 7-point scale and it predicts the mean vote Mediterranean people might give to judge the thermal quality of an outdoor environment, based on the following expression (Eq. (9)):

$$MOCI = -4.068 - 0.272\cdot w_s + 0.005\cdot RH + 0.083\cdot MRT + 0.058\cdot T + 0.264\cdot I_{cl} \quad (9)$$

where the parameters affecting the MOCI index value are wind speed ($w_s$), relative humidity (RH), mean radiant temperature (MRT), air temperature (T), and clothing insulation ($I_{cl}$).

## 4. Results of the experimental analysis

### 4.1. Urban heat island, air and surface temperatures and relative humidity

Trends of air temperature (T) and relative humidity (RH) values monitored in all the case study areas, for the two selected measurement periods, are reported in Fig. 5.

The esults of the monitoring campaign highlight that the role of the solar radiation directly reaching the sensors is non-negligible in the SG area, where there are no urban obstacles and the highest values of maximum daily air temperature are registered. At the same time, lower temperature values are detected in SG during night. This result is consistent with the analysis of data collected by the weather stations located in SG and SB during whole summer 2015, when a mean nightly air temperature difference between the suburban green and built area of about −0.8 °C was detected. Moreover, by comparing suburban to urban areas, characterized by reduced vegetated area, it is evident how built surfaces influence microclimate parameters acting as hygro-thermal buffer due to their storage capability. In particular, the lowest daily temperature fluctuations are registered in the two urban areas presenting the highest building density and, therefore, the lowest sky-view factor. Such configuration implies (i) limited thermal exchange with the sky and (ii) larger amount of re-emitted infrared radiation tripped within the urban canyon. The lowest night radiative cooling is registered in the recent urban neighborhood (UR area) and the historical one (UH area), when maximum discrepancies of 2 °C and 5 °C, respectively, occurred compared to the suburban green area (SG area). Additionally, Fig. 5, as expected, stresses the inverse correlation between temperature and relative humidity values. Nevertheless, as highlighted in Table 3, the weakest correlation occurs in UH area, i.e. the case with the highest building density, where the relative humidity trend presents one-hour delay compared to the temperature curve.

By comparing the values collected in the four case study areas, the influence of the built environment local boundary characteristics seems to be more significant in the UH area. In fact, the highest building density and consequent lowest sky-view factor generate the smallest radiative heat flux exchange with the sky and the largest amount of radiative fluxes from built surfaces, responsible for the nighttime overheating.

Furthermore, differences in terms of air temperature are shown in

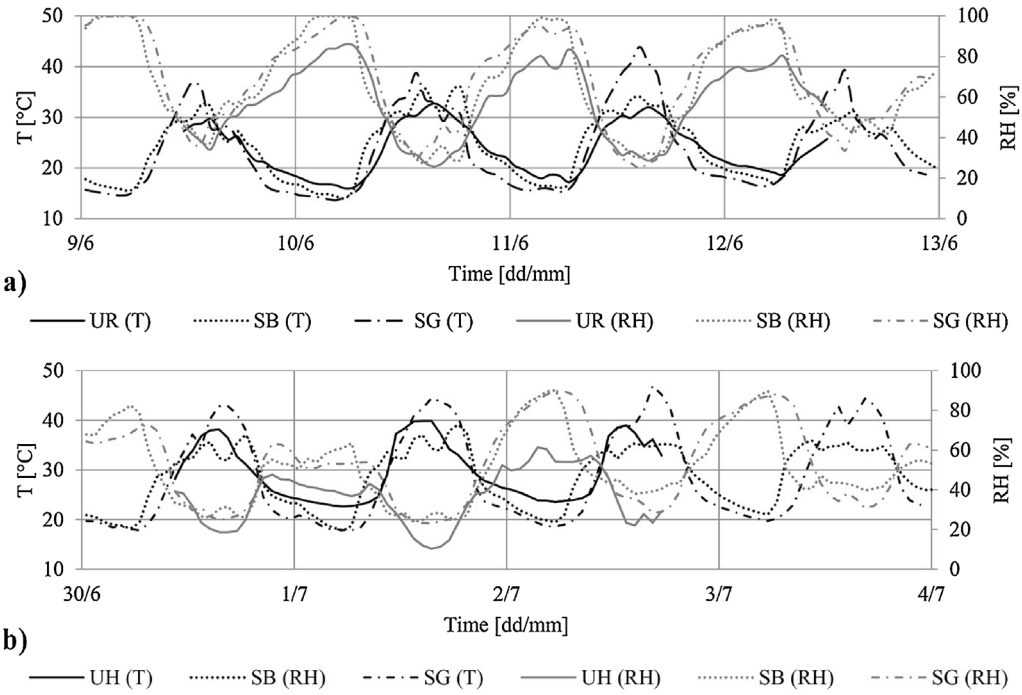


**Fig. 5.** Comparison (a) between UR, SB, and SG during the period June 9th-12th, 2015 and (b) between UH, SB, and SG areas during the period June 30th-July 3rd, 2015, in terms of average hourly air temperature and relative humidity.

Fig. 6, which depicts the mean hourly variation detected between the two urban areas and the suburban green area during the whole monitoring period. Graphs show the non-negligible UHI intensity in the two urban areas. In fact, during the daytime (from 6:00 a.m. to 8:30 p.m.), i.e. in presence of direct solar radiation, the suburban green area is characterized by higher temperatures due to the higher SVF and, therefore, to the stronger impact of the more accessible short-wave solar radiation. Nevertheless, during the nighttime, significantly higher and more constant air temperatures are measured in urban areas compared to the suburban green area, especially in the historical urban area. Therefore, the UH area is characterized by the most intense urban heat island phenomenon due to the reduced SVF, high building density, and lack of vegetated surfaces.

A positive linear correlation between air and surfaces temperatures (sT) is also detected during the night, i.e. from 8:30 p.m. to 6:00 a.m., when no solar radiation is available (Fig. 7a). The correlation is stronger in the historic urban area (i.e. $R^2$ up to 0.99), where the reduced sky-view factor is able to maximize the long-wave radiative thermal exchange of built surfaces. Moreover, in both urban scenarios, i.e. the UH and UR areas, no significant differences are detected considering the different analyzed components. In fact, even if thermal properties of each specific material are different, dimensions of the monitored surface and the effect of ageing led to similar thermal behavior. For instance, by considering the UH area, even if wood has lower thermal conductivity and emissivity compared to travertine stone, the volume of the wooden window frame is rather lower than the volume of the thick stone wall. Therefore, negligible differences are detected in processes of heating and cooling up of their surfaces. On the contrary, during the daytime, i.e. from 11:00 a.m. to 5:00 p.m., the correlation between air and surfaces temperatures is reduced (Fig. 7b). In particular, no linear correlation is detected at high temperatures (> 35 °C) with reference to the wooden horizontal surface (UH area). This effect is mainly due to the surface exposure, since in central hours of the day the solar radiation is almost perpendicular to that surface.

### 4.2. $CO_2$ concentration

In this section, the $CO_2$ concentration level in the two case study urban environments, i.e. recently developed neighborhood (UR area) and historic area (UH area), was analyzed (Figs. 8 and 9) and possible correlations with urban overheating were investigated. In particular, the correlation between $CO_2$ concentration and the main microclimate parameter characterizing local urban microclimate, i.e. outdoor air temperature, was assessed (Fig. 8). The aim of this analysis was to evaluate the coexistence of two issues affecting outdoor air quality (Ward et al., 2015), namely urban overheating and $CO_2$ emissions. Moreover, Fig. 9 shows the daily trend of hourly mean values of $CO_2$ concentration, obtained as the average of the data collected during days of the whole monitoring period. Daily values are averaged in order to dampen down the influence of temporary phenomena strongly affecting the collected data.

Results show (i) a daily variation of the parameter strongly related to the air temperature and (ii) a higher background $CO_2$ level in the urban recent neighborhood (UR area) compared to the historic urban area (UH area). The first statement seems to be due to the influence of solar-inducted convective mixing that plays an important role on the air flux, especially in absence of a strong seasonal wind. In fact, during the monitoring period, in both the urban cases the collected wind speed values were always below 2 m/s and were lower in the UH area, where buildings density is higher. The plotted data show a linear inverse correlation between temperature and $CO_2$ concentration at local scale.

The second statement underlines the influence of anthropogenic activities on local $CO_2$ concentration. In fact, for both the monitored areas, which are far from the industrial zone of the city and therefore from strong point sources of greenhouse gases emissions, the most important source of $CO_2$ is represented by vehicles traffic and cooling systems emissions, in the monitored summer period. While vehicles

**Table 3**
Linear correlation between T and RH for each assessed scenario.

| Case study | $R^2$ | |
|---|---|---|
| | 09–12/06/2015 | 30/06–02/07/2015 |
| UR | 0.96 | – |
| SB | 0.96 | 0.75 |
| SG | 0.98 | 0.73 |
| UH | – | 0.66 |

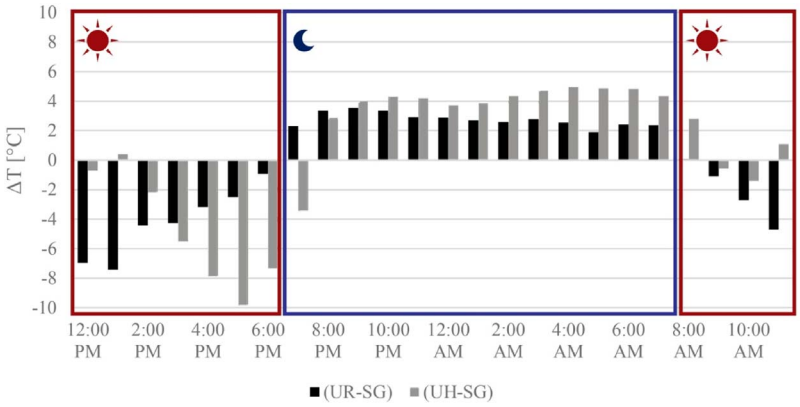


**Fig. 6.** Difference of the mean hourly air temperature, evaluated during the monitoring period, in UH and UR area with respect to SG.

circulation inside the historical city center is allowed only for residents, the monitoring station in the UR area is facing a congested street connecting the lower and the upper part of the city. As a consequence, a different level of $CO_2$, clearly represented by the vertical shift of curves trend in Fig. 9, was detected in the two areas.

## 5. Results of the numerical analysis

### 5.1. Calibration of the model

This section concerns the description of results of the calibration procedure of the model of the historic urban area, i.e. UH area. The aim of this analysis is to assess the local urban microclimate and, therefore, the outdoor thermal comfort conditions in the case study historic area in a representative summer and winter day, since the monitored data highlighted the presence of summer nocturnal UHI phenomenon in the area.

According to previous studies (Kong et al., 2016) the validation of the model was performed by comparing observed and simulated air temperature and relative humidity profiles. The graph in Fig. 10a compares the simulated time profiles of temperature and relative humidity extracted at point A (Fig. 4d) to those collected during the monitoring campaign by the hygrothermal sensor located in the same position. The differences among the simulated and monitored parameters are reported in Fig. 10b. The software seems to overestimate the nighttime cooling in the area, with a maximum discrepancy of −0.9 °C at 7:00 a.m., and air temperature values during the middle hours of the day, when the greatest difference of +2.4 °C is observed at 4:00 p.m.

Moreover, the calculated calibration indexes are summarized in Table 4. Obtained values are considered acceptable according to literature (Salata et al., 2016a) (i.e. mean value of RMSE and Willmott's index equal to 1.84 °C and 0.78, respectively, for calibrated models).

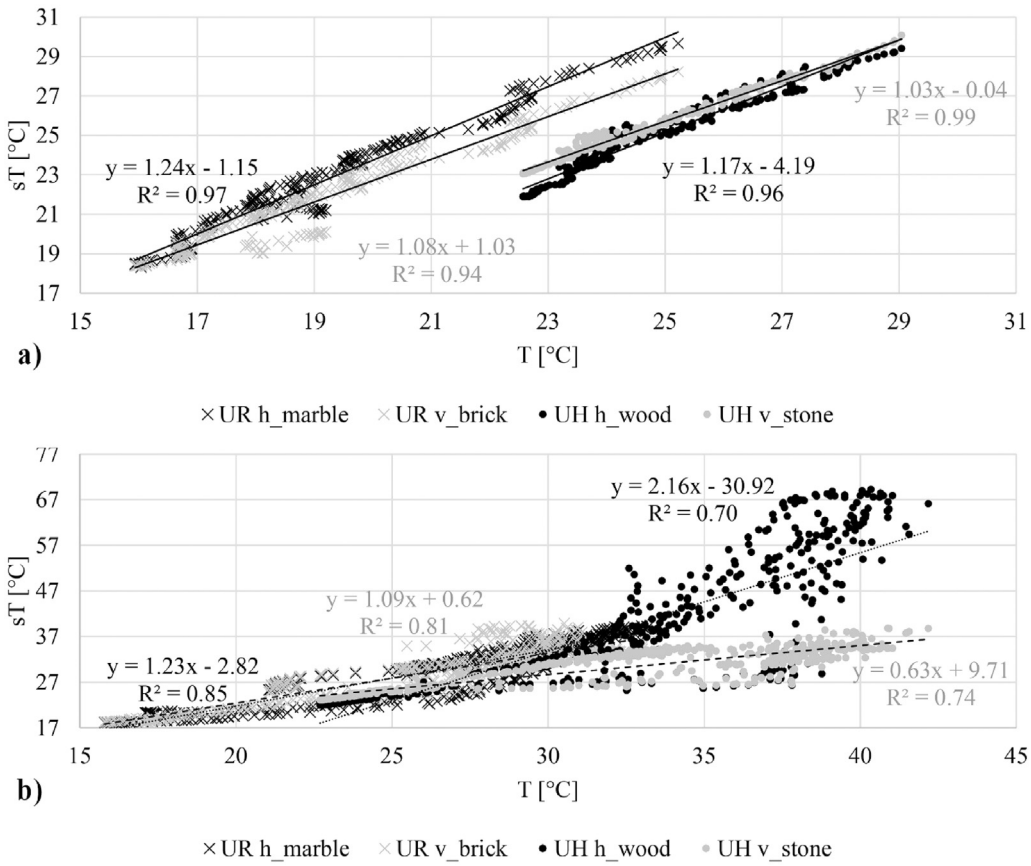


**Fig. 7.** Dispersion graph of monitored surfaces temperatures vs. air temperature during (a) the nighttime and (b) the whole day for the urban cases.

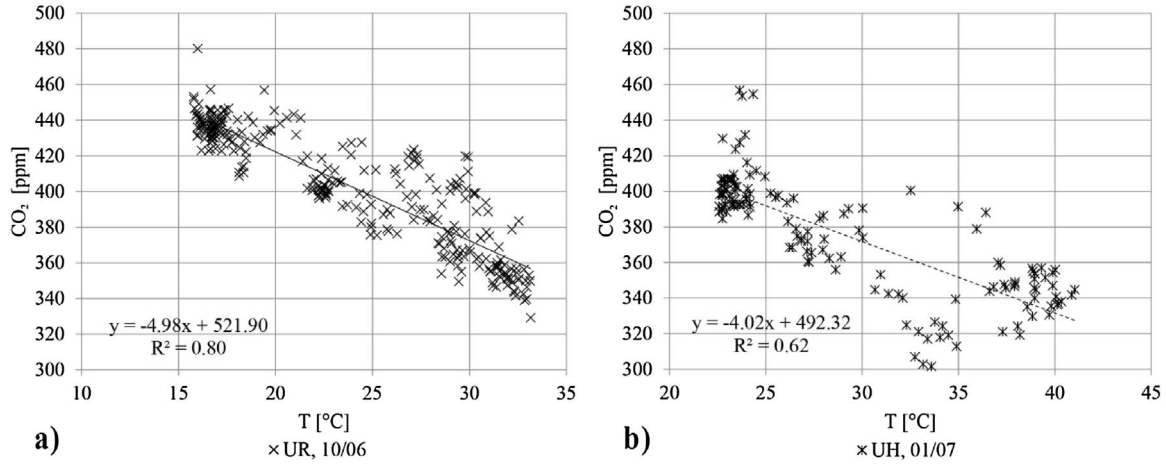


**Fig. 8.** $CO_2$ concentration vs. outdoor air temperature for (a) UR and (b) UH areas respectively.

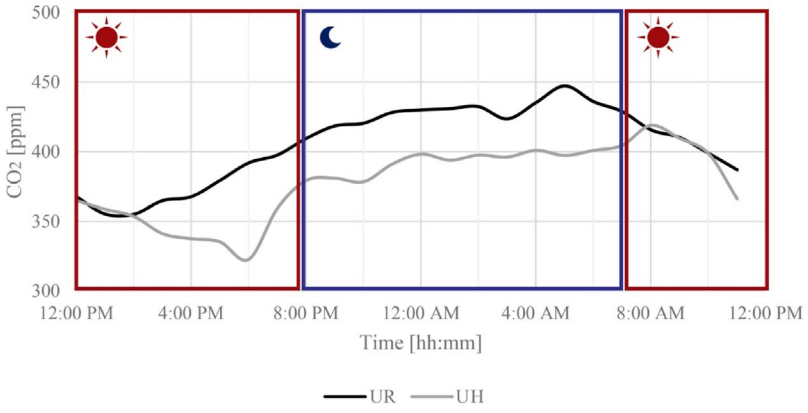


**Fig. 9.** Comparison between the $CO_2$ concentration daily profile in the two the urban areas.

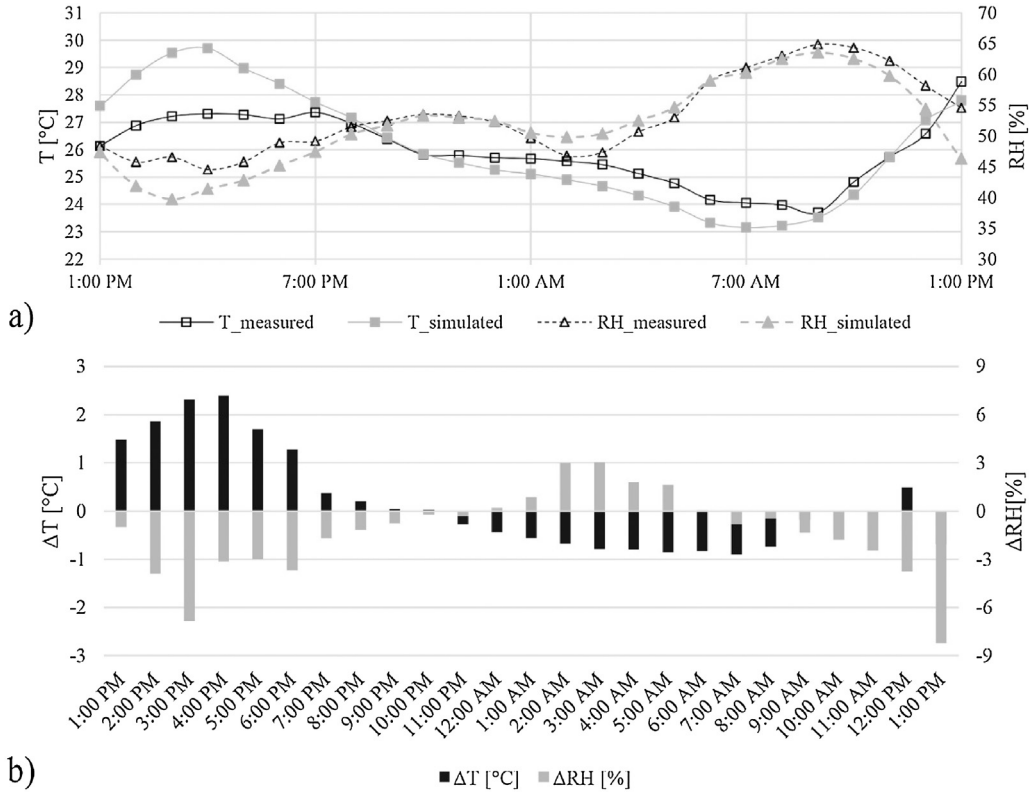


**Fig. 10.** Validation of the model in terms of air temperature and relative humidity.

**Table 4**
Calibration parameters.

| Parameter | T | RH |
|---|---|---|
| MBE | 0.82 °C | 2.21% |
| RMSE | 1.05 °C | 2.96% |
| Willmott's index | 0.71 | 0.79 |

**Table 5**
Characteristics of the two selected points in the model.

| | Location | SVF | Access to direct solar radiation |
|---|---|---|---|
| Point 1 | 3/4 m distant from the E-W/N-S oriented walls, respectively above the asphalt pavement | 0.15 | 12:00–2:00 p.m. |
| Point 2 | | 0.51 | 3:00–8:00 p.m. |

### 5.2. Local microclimate variations in the historic area

This section reports the results of the numerical analysis of the UH area model.

In particular, the daily weather profiles of two representative days in summer and winter (i.e. July, 15th and January, 15th) were selected. The analysis was carried out by using the TMY (Typical Meteorological Year) for the city of Perugia, which refers to a 20-year measurement period, i.e. 1951–1970 (U.S. Department of Energy, Energy Efficiency and Renewable Energy, 2014).

The data for the outdoor thermal comfort analysis were extracted at 1.5 m from the ground in two different points of the model (Fig. 11), which were selected because of their different characteristics in terms of location, SVF, and access to direct solar radiation (Table 5).

In the following sub-sections, results of the microclimate simulation of the historic area are reported for the selected summer and winter day.

#### 5.2.1. Summer conditions

Fig. 12a shows the trend of outdoor air temperature and relative humidity in the two selected points of analysis (Fig. 11), i.e. point 1 (pt1) and point 2 (pt2), in summer conditions.

A maximum outdoor air temperature equal to 26 °C is detected at pt2 at around 3:00 p.m. At the same time the outdoor air temperature detected at pt1is slightly lower, i.e. by 1 °C compared to pt2, due to the lower sky-view factor and, therefore, reduced access to direct solar radiation. Accordingly, point 1 presents slower night cooling process, i.e. cooling rate of 0.56 °C/h compared to 0.77 °C/h of point 2.

Negligible differences are detected between the two points in terms of relative humidity, which ranges between 40% and 60%.

Results in terms of reflected solar radiation and mean radiant temperatures are reported in Fig. 12b. Despite reflected solar radiation trends are almost equal in the two points, two different peaks of mean radiant temperature (i.e. over 50 °C) are registered at around 1:00 p.m. and 3:00 p.m. for pt1 and pt2, respectively. In fact, the two points are

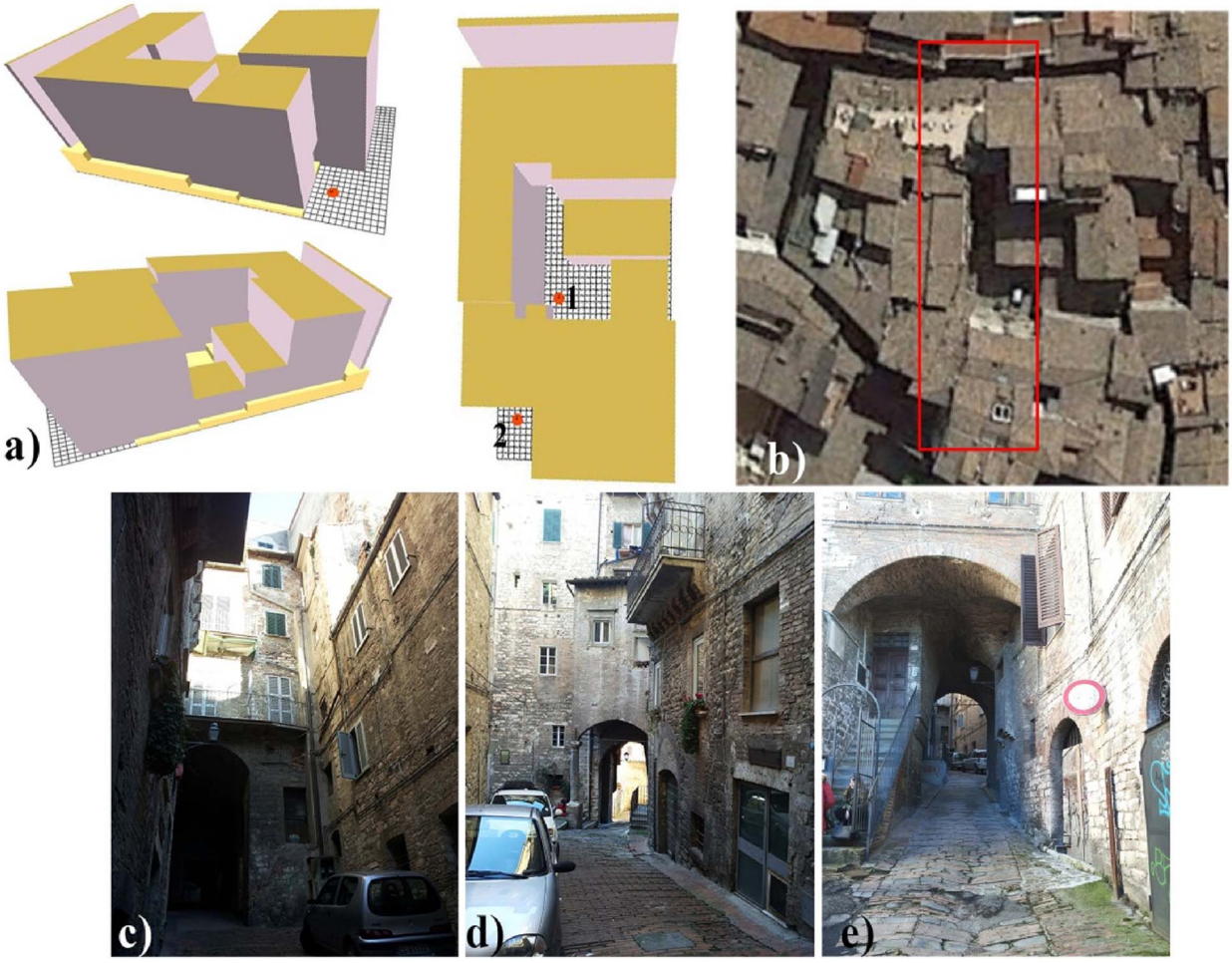


**Fig. 11.** (a) Views of the 3D model and indication of the analysis points 1 and 2; (b) location of the modeled area within the historical urban context and real views of the area from (c,d) point 1 and (e) point 2.

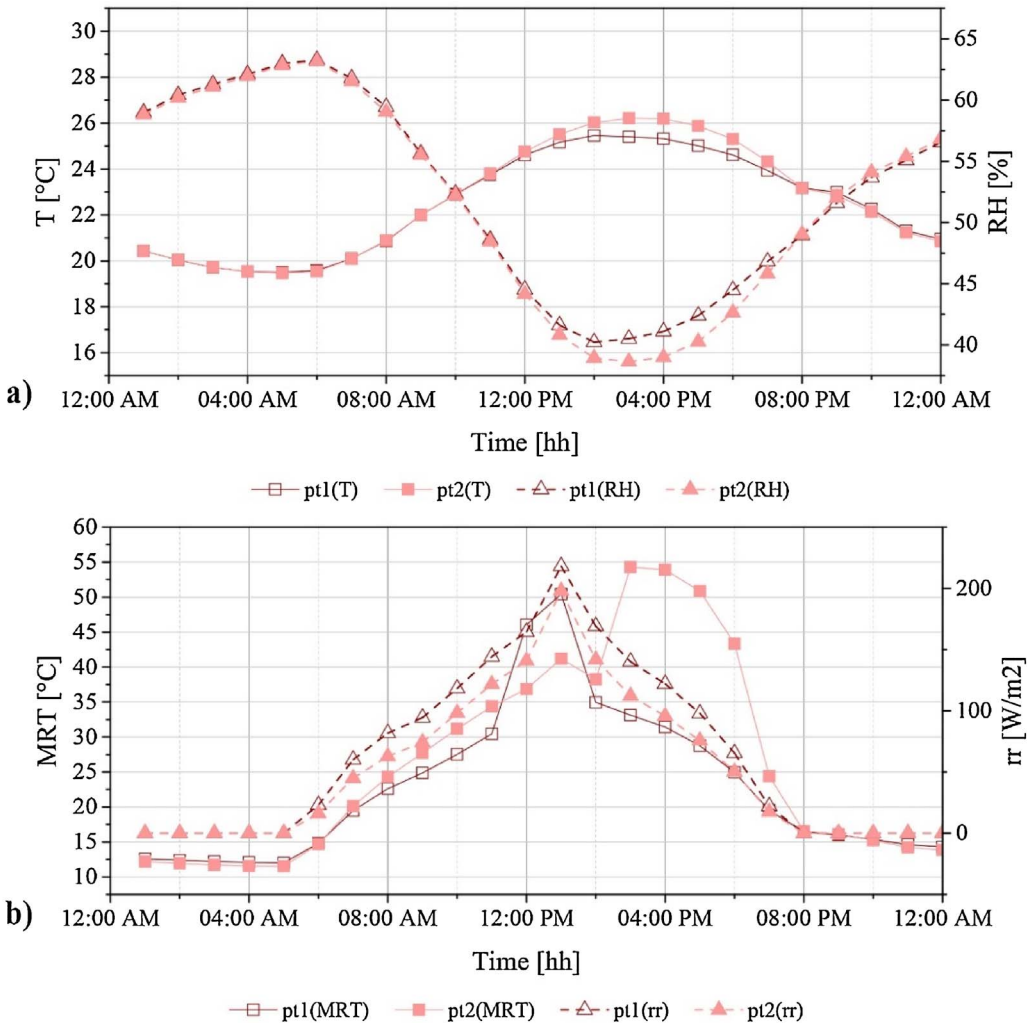


**Fig. 12.** (a) Outdoor air temperature and relative humidity and (b) mean radiant temperature and reflected solar radiation daily trend at point 1 and 2 in the selected summer day.

reached by direct solar radiation in two different times of the day, due to different multiple obstructing buildings responsible for shading the selected points. Moreover, paving materials present non-negligible role. Higher mean radiant temperature values are detected in proximity of the asphalt pavement (point 2), which reaches the highest surface temperature during the day, i.e. around 35 °C. Therefore, it is able to re-emit the highest amount of long-wave radiations during night.

#### 5.2.2. Winter conditions

Fig. 13 reports daily trends of the main monitored microclimate parameters in point 1 and 2 for the selected winter day.

As shown in Fig. 13a, outdoor air temperatures vary between a minimum of 3.5 °C (at 5:00 a.m.) and a maximum of about 6 °C (at 3:00 p.m.). Relative humidity values range from 74% up to 84%. Consistently with measurements, simulations confirm the inverse correlation between air temperature and relative humidity. Significant differences are detected between pt1 and pt2 in terms of outdoor air temperature and relative humidity values (Fig. 13a).

On the contrary, unlike summer results, in the winter scenario negligible differences are detected between pt1 and pt2 in terms of reflected solar radiation and mean radiant temperature trends (Fig. 13b). This is due to the sun low-height and less intense and durable solar radiation in winter, that almost never reach both points due to high buildings density of and low sky-view factor. Maximum values of mean radiant temperature of about 10 °C are detected in both points.

### 5.3. Outdoor environmental comfort in summer and winter conditions

In this section, the comfort analysis is performed in terms of PET (Physiological Equivalent Temperature) (Chirag and Ramachandraiah, 2010), PMV (Mean Predicted Vote) (Yang et al., 2013), and MOCI (Mediterranean Outdoor Comfort Index) (Matzarakis et al., 2007).

Summer daily trends of all the considered comfort indexes are reported in Fig. 14. By comparing the MOCI and PMV indexes, it is evident how during the day MOCI values stay (i) closer to the neutral condition, i.e. around 0, and (ii) for a longer period compared to PMV values. More in detail, MOCI is kept between +1 and −1 from the sunrise until the sunset, i.e. from 7:00 a.m. to 7:00 p.m. However, when points are reached by direct solar radiation, i.e. from 12:00 p.m. to 1:00 p.m. in pt1 and from 2:00 p.m. to 6:00 p.m. in pt2, higher MRT values are detected. Similarly, PMV assumes values higher than +1 during daytime when points are reached by direct solar radiation. Nevertheless, PMV maintains values lower than −1 for a 2-h longer period after sunset. Furthermore, maximum values of both indexes are similar in the two points, i.e. +1.9 (MOCI) and +1.7 (PMV) in point 1 and +2.3 (both) in point 2, while a consistent difference is detected between their minimum values, i.e. −1.5 (MOCI) and −2.4 (PMV) in both the points at 5:00 a.m.

Moreover, Fig. 14 shows the time profile of the PET calculated by considering a standard man (i.e. 35 years old, 1.75 h, 75 kg, clo of 0.5, and 80 W of activity) for the selected summer day. The trend is similar to those ones of the above analyzed indexes, and implies discomfort conditions for pedestrians in the two selected points after 1:00 p.m.

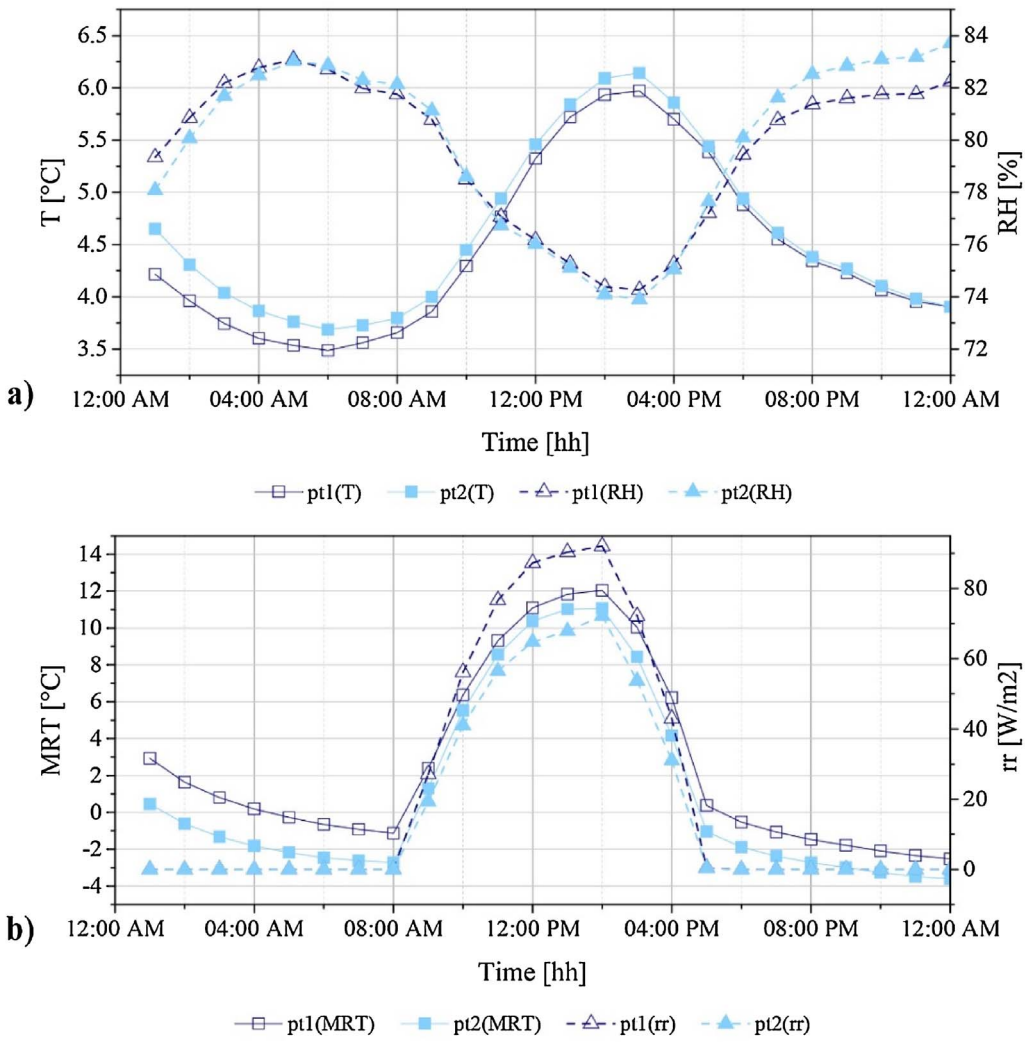


**Fig. 13.** (a) Outdoor air temperature and relative humidity and (b) mean radiant temperature and reflected radiation daily trend at point 1 and 2 in the selected winter day.

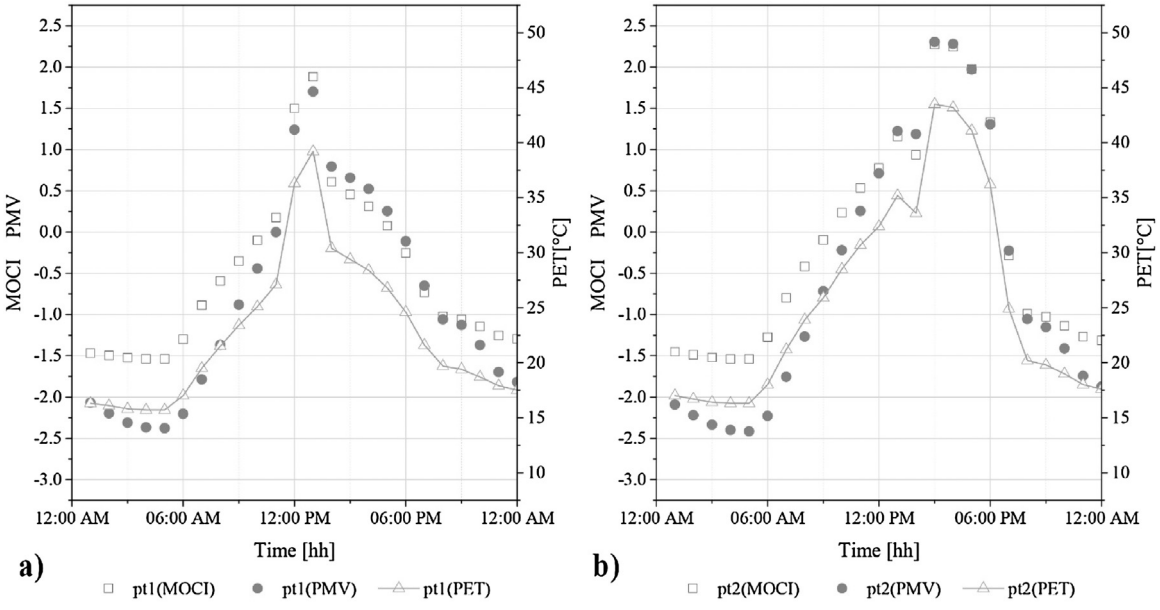


**Fig. 14.** MOCI, PMV, and PET daily trend at (a) point 1 and (b) point 2 in the selected summer day.

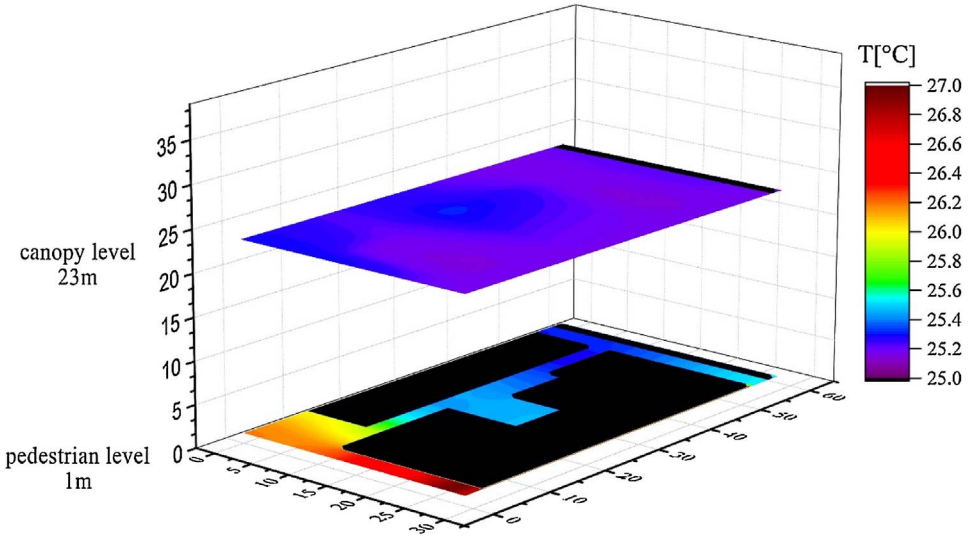


**Fig. 15.** Outdoor air temperature spatial distribution at canopy and pedestrian level at 2:00 p.m. in the selected summer day.

until the sunset, i.e. 7:00 p.m. In particular, extremely hot thermal perception for pedestrians is detected in point 2, the one presenting the highest SVF.

The spatial distribution of outdoor air temperature at canopy level, i.e. at 1 m above buildings roof, and at pedestrian level, i.e. 1 m above ground, is, therefore, analyzed (Fig. 15) for the selected summer day at 2 p.m., when the considered parameter reaches its maximum.

At canopy level, the air temperature distribution is found to be generally homogenous, i.e. with variability of about 0.15 °C, while at pedestrian level non-negligible air temperature fluctuation is detected. In particular, consistently with the previous results, a significantly higher temperature, i.e. +0.7 °C, is registered in pt2, situated above the asphalted area, with respect to pt1, located in close proximity to the building wall. By observing the temperature distribution at pedestrian level, generally higher temperatures are detected in the western part of the area, which is at lower height. In fact, between the western and the eastern side of the street there is a 5-m altitude difference. The stagnation of high temperatures in the lower part of the area is also due to the absence of strong winds, since mean wind speed is lower than 0.8 m/s.

Maps in Fig. 16 show the mean radiant temperature spatial distribution within the historic case study area. Results are reported both at 1:00 p.m., when the short-wave solar radiation contribution is maximum, and at 9:00 p.m., when the long-wave radiation from built surfaces has its strongest effect.

During the daytime (Fig. 16a), a generally non-homogenous distribution of the mean radiant temperature is detected, with discrepancies up to 27 °C between the sunny and shaded areas. Furthermore, highest MRT values are observed in the low part of the model, i.e. west side of the street, where also the highest air temperature values are detected.

During night (Fig. 16b), less significant mean radiant temperature differences are observed, i.e. about 4 °C. Nevertheless, it can be noticed that the west side of the area, which is covered with traditional asphalt, presents the highest mean radiant temperature values both during daytime and nighttime, where there is not solar radiation available.

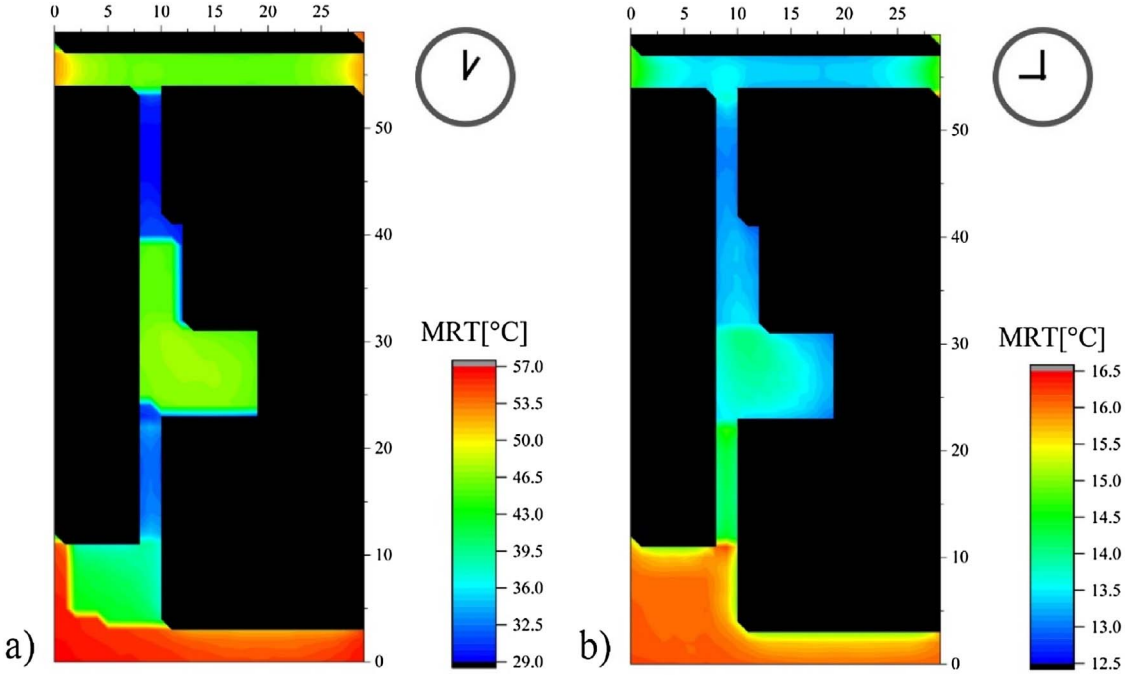


**Fig. 16.** Mean radiant temperature spatial distribution at pedestrian level in the selected summer day at (a) 1:00 p.m. and (b) 9:00 p.m.

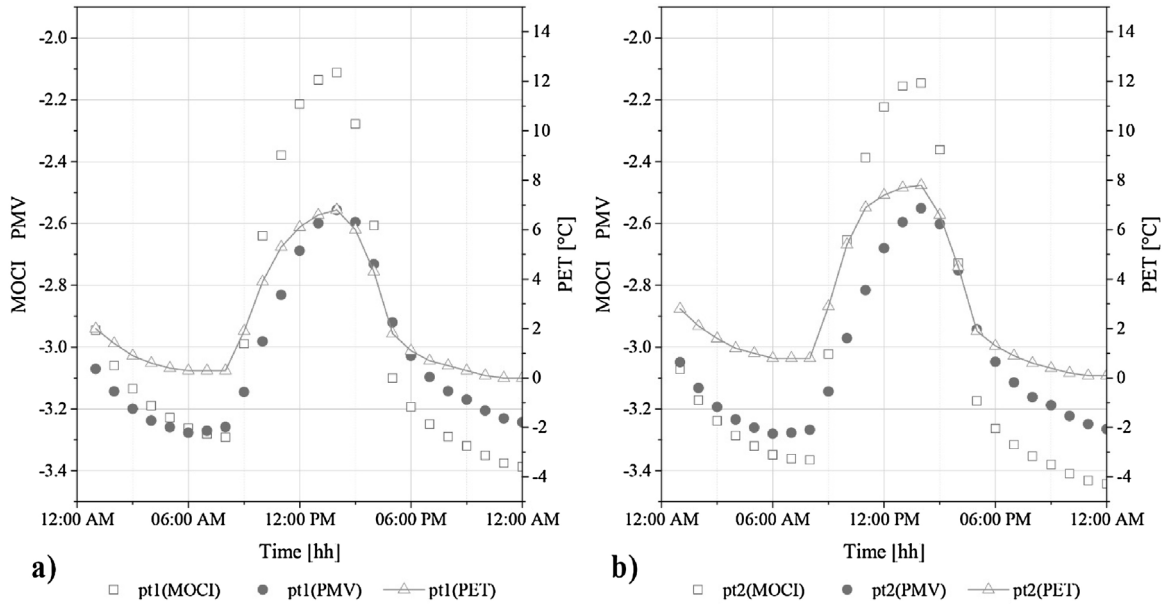


**Fig. 17.** MOCI, PMV, and PET daily trends at (a) point 1 and (b) point 2 in the selected winter day.

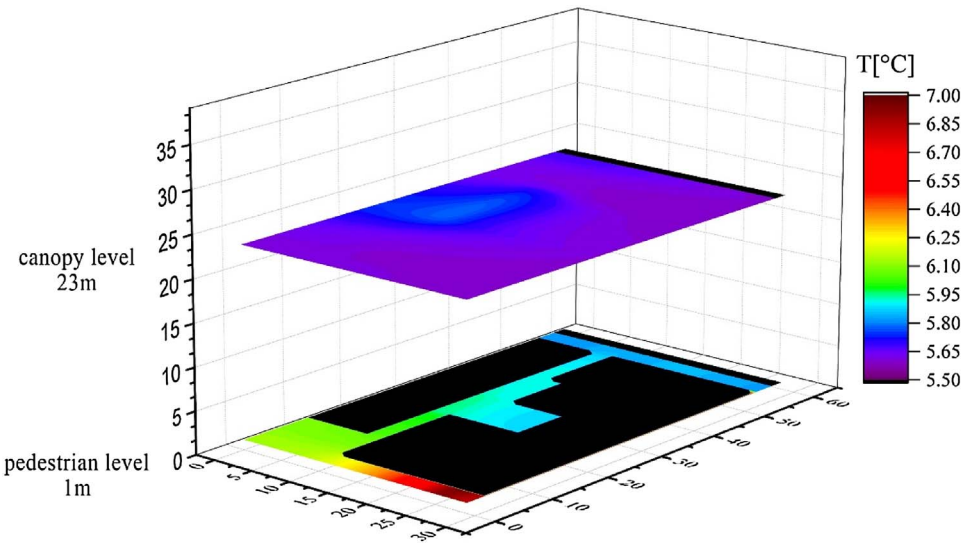


**Fig. 18.** Outdoor air temperature spatial distribution at canopy and pedestrian level at 2:00 p.m. in the selected winter day.

This is mainly motivated by the higher surface temperatures achieved.

The winter daily profile of calculated comfort indexes is shown in Fig. 17. Insignificant variations are detected between pt1 and pt2 in terms of MOCI and PMV. During the daytime, MOCI presents values closer to the neutral condition of 0 compared to PMV, even if it never exceeds the value of −2. However, during nighttime MOCI assumes values of higher thermal discomfort with respect to PMV.

On the other hand, the trend of PET in the selected winter day, calculated considering a clo of 1.2 and 80 W of activity, is different between the two points. In detail, during the daytime, higher PET values are registered in point 2, corresponding to a maximum discrepancy between the points equal to +1.6 °C at 11:00 a.m. In fact, above the asphalted area, PET values range from 0.1 °C (nighttime) to 7.8 °C (daytime) for a standard man.

The spatial distribution of outdoor air temperature at canopy level and at pedestrian level for the selected winter day is shown in Fig. 18, when the maximum air temperature is detected, i.e. at 2:00 p.m. At pedestrian level, i.e. at 1 m above ground, a wider temperature fluctuation can be detected with a difference of 1.2 °C between the western and eastern side of the area.

As for the spatial variation of mean radiant temperature values, Fig. 19 shows maps at 1:00 p.m. and 9:00 p.m. in the selected winter day. In absence of solar radiation negligible differences are detected in the spatial distribution of mean radiant temperature, while during daytime a significant temperature gap is detected between pt1 and pt2, i.e. equal to around 2 °C. This is motivated by the fact that in absence of short-wave solar radiation, the impact of surrounding built surfaces plays a major role in terms of long-wave radiation. Therefore, point 1 shows higher mean radiant temperature values compared to point 2, which presents higher sky-view factor and is less affected by long-wave radiation phenomena.

## 6. Discussion and implications of the results

In summary, the present study highlights the following main findings:

1. The occurrence of a non-negligible local UHI phenomenon within the context of the historical area. In fact, a night urban heat island intensity up to 5 °C was measured in the urban historic area (UH)

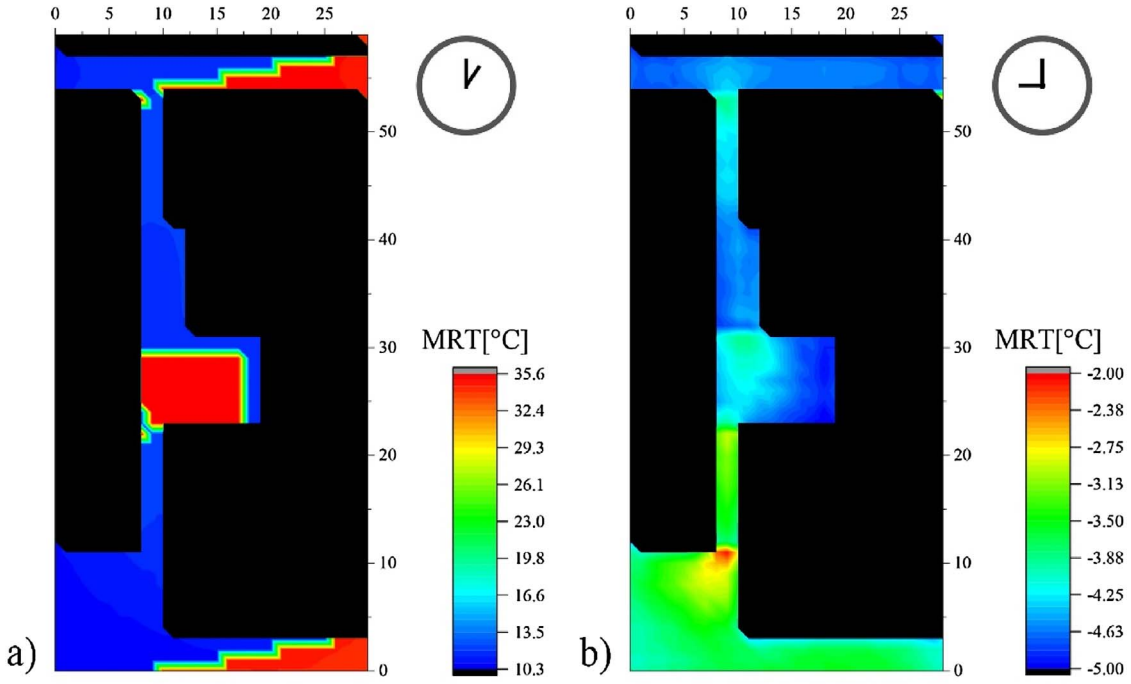


**Fig. 19.** Mean radiant temperature spatial distribution at pedestrian level in the selected winter day at (a) 1:00 p.m. and (b) 9:00 p.m.

compared to the surrounding suburban green areas. For this reason, citizens and users living in historic areas are potentially more vulnerable to UHI related issue. Consequently, they should be more aware about the negative effects on the outdoor thermal comfort and human health generated by such local overheating phenomenon.

2. However, such historic city center is less affected by other air quality issues, since mean $CO_2$ daily concentration lower than 400 ppm was registered in the historic area, which is lower compared to that one measured in the more recent urban neighborhood (UR). Despite the UHI occurrence, the air quality is more acceptable in the monitored historic area compared to the other urban area assessed, meaning that the anthropic overheating is mainly imputable to buildings heat storage and release.

Therefore, the present research study shows the urgent need for information campaigns among the citizens of such historic areas affected by UHI. In fact, such people, of which a large majority is constituted by old people living in ancient and low-energy-quality constructions, are usually neither provided with cooling or any active control systems. Therefore, they are much more vulnerable to such local climate phenomena generating serious health problems related to the overheating risk. A dedicated educational campaign should be carried out in historical centers affected by UHI in order to engage the community to apply simple strategies at inter-building scale for counteracting such phenomenon.

Moreover, this study highlights the need for a standardization of the regulations about the outdoor thermal comfort conditions of pedestrians, similar to those for indoor thermal comfort. In fact, up to now, several multiple indexes characterized by different physical meanings and referring to different boundary conditions (e.g. PET, MOCI, PMV, etc.) are available, but they are not mutually consistent. Moreover, they are not yet regulated by national and/or international acknowledged standards.

## 7. Conclusions

Local urban microclimate phenomena such as Urban Heat Island can considerably affect the quality of outdoor built environments from the citizens' perspective, since they represent a serious threaten to human health in terms of overheating risk. Moreover, their effect can significantly vary due to local boundary conditions, e.g. presence of vegetation, urban density and configuration, surface materials, etc.

In this paper, the analysis of the impact of different boundary conditions on the local microclimate at district scale, characterizing historical city centers situated at the top of hills, is performed through combined experimental and numerical analysis. Four areas located within the same city in central Italy, but characterized by different building density, constructions materials, and amount of greenery, were continuously monitored during summer 2015. The main microclimate parameters in each area were characterized and compared. Finally, the numerical modeling of the historical area, which was detected to be the one majorly affected by UHI, was carried out to assess its microclimate in summer and winter and to analyze pedestrians' thermal comfort conditions.

The research was aimed at investigating the local microclimate conditions in such typical hilly historic district, where high construction density and low SVF mainly affect pedestrians' thermal perception. Nevertheless, they are less subjected to low air quality levels or anthropogenic heat release caused by traffic and industrial activities, such as classic new urban developments. In this view, the purpose of the study is to fill the gap in UHI research, where flat urban areas, both coming from historical and new developments, are mainly investigated, while ancient urban layouts are weakly studied. However, they represent the typical architectural layout of Middle-Age cities constructed over the top of hills for military protection purpose and they often host cities core in Mediterranean and, more in general, European countries.

The experimental campaign allowed to detect non-negligible discrepancies in the local climate of the different monitored neighborhoods, directly imputable to spatial and architectural constrains of the surrounding environment. In particular, the urban historical area (UH) appears to be affected by the highest local urban heat island during night, with a maximum air temperature discrepancy of about 5 °C compared to the suburban green area (SG). Therefore, despite the high thermal mass of its ancient structures, the historic area does not show a better outdoor thermal quality. This is mainly due to the lack of greenery in this area, which implies that all the energy fluxes entering the system are converted to sensible heating of the environment.

Moreover, both the historical and more recent urban areas present the lowest daily fluctuation in outdoor air temperature. This is due to the high density and massive configuration of buildings and, therefore, the low sky-view factor leading to limited solar access during the day and reduced re-emitted long-wave radiations to the sky at night.

The numerical analysis showed results consistent with the experimental data. The potential of local constrains, such as high buildings density and surrounding built surfaces, in generating discrepancies in terms of outdoor air and mean radiant temperature mainly in summer was highlighted. In fact, the local microclimate in the point characterized by reduced access to solar radiation during the day is much more affected by mutual long-wave radiation effects of surrounding buildings. Therefore, it presents slower night cooling process compared to the point presenting the highest SVF. However, the thermal comfort analysis showed that the zone with higher sky-view factor and covered with asphalt presents the highest mean radiant temperature values both during daytime and nighttime, where there is not solar radiation available. Therefore, it is characterized extremely hot thermal perception for pedestrians.

The achieved results demonstrated the non-negligible impact of local boundaries and constrains of the surrounding context on the local microclimate at settlement level. Moreover, the detailed analysis of the environmental parameters and citizens' thermal comfort conditions within the historical area confirmed that local boundaries must necessarily be taken into account while assessing the quality of outdoor urban environments, since they are able to significantly affect the thermal comfort of pedestrians. Moreover, the achieved results highlight the need to provide solutions for reducing the outdoor overheating risk for pedestrians and, more in general, for citizens in historic city centers, which are typically not well prepared to be resilient to local climate change phenomena such as UHI. Therefore, information and educational campaigns and dedicated surveys should be carried out to engage the community and make people more aware about the multiple possible solutions available to counteract such phenomena. In fact, the role of citizen is fundamental to make the pre-selected countermeasures to UHI phenomena more effective in specific urban areas.

Moreover, the analysis of local boundary conditions (i) allowed to select the most effective solutions for mitigating local phenomena affecting human comfort conditions and (ii) helps to predict the realistic effect of such strategies in improving the local microclimate. In particular, for the case study historical area, three main strategies could be implemented as suitable solutions to mitigate the local environment and improve thermal comfort, according to the results of the analysis performed:

- introduction of greenery, where possible, also by replicating green walls, that already exist close to the case study area;
- application of cool materials with the same aesthetic appearance of the historical ones but with higher solar reflectance capability, both at roof and pavement level;
- integration of PCMs within building envelope in order to improve its thermal storage capability.

Future developments of the study will concern the evaluation of the effectiveness of different Urban Heat Island mitigation strategies, specifically selected as "tailored" for the case of historic areas, where buildings are usually subjected to many constraints due to their high cultural heritage value. The final aim will be to provide reliable information to support designers, policy makers and urban planners in the development of in-field mitigation strategies and policies to improve citizens' quality of life.

## References


ANSI/ASHRAE (2002). *ASHRAE Guideline 14–2002 Measurement of Energy and Demand Savings, vol. 8400*, Ashrae170.

Alvarez, S. (2001). Experimental work and analysis of confined urban spaces. *Solar Energy*, *70*, 263–273.

Association of German Engineers (1998). *Methods for the human-biometeorological assessment of climate and air hygiene for urban and regional planning. Part I: Climate. VDI guideline 3787*.

Bagiorgas, H. S., & Mihalakakou, G. (2016). On the influence of the urban heat island on the cooling load of a school building in Athens, Greece. *Journal of Atmospheric and Solar-Terrestrial Physics*, *138–139*, 179–186.

Bianchi, F., Pisello, A. L., Baldinelli, G., & Asdrubali, F. (2014). Infrared thermography assessment of thermal bridges in building envelope: Experimental validation in a test room setup. *Sustainability*, *6*(10), 7107–7120.

Busato, F., Lazzarin, R. M., & Noro, M. (2014). Three years of study of the Urban Heat Island in Padua: Experimental results. *Sustainable Cities and Society*, *10*, 251–258.

Cheung, T. C. T., Schiavon, S., Gall, E. T., Jin, M., & Nazaroff, W. W. (2017). Longitudinal assessment of thermal and percieved air quality acceptability in relation to temperature, humidity, and CO2 exposure in Singapore. *Building and Environment*, *115*, 80–90.

Chirag, D., & Ramachandraiah, A. (2010). The significance of Physiological Equivalent Temperature (PET) in outdoor thermal comfort studies. *International Journal of Engineering Science and Technology*, *2*, 2825–2828.

Consuegra, L. G., & Matzarakis, A. (2016). Spatial-temporal study on the effects of urban street configurations on human thermal comfort in the world heritage city of Camagüey-Cuba Jose Abel Rodríguez Algeciras. *Building and Environment*, *101*, 85–101.

ENVI-met software, 2017, Köppen-Geiger, 2017, http://www.model.envi-met.com.

Emmanuel, R. (2005). Thermal comfort implications of urbanization in a warm-humid city: the Colombo Metropolitan Region (CMR), Sri Lanka. *Building and Environment*, *40*, 1591–1601.

Galli, G., Vallati, A., Recchiuti, C., de Lieto Vollaro, R., & Botta, F. (2013). Passive cooling design options to improve thermal comfort in an Urban District of Rome, under hot summer conditions. *International Journal of Engineering and Technology*, *5*, 4495–4500.

Georgakis, Ch., Zoras, S., & Santamouris, M. (2014). Studying the effect of cool coatings in street urban canyons and its potential as a heat island mitigation technique. *Sustainable Cities and Society*, *13*, 20–31.

Giridharan, R., Lau, S. S. Y., Ganesan, S., & Givoni, B. (2007). Urban design factors influencing heat island intensity in high-rise high-density environments of Hong Kong. *Buildings and Environment*, *42*, 3669–3684.

Grimmond, C. S., King, T., Cropley, F., Nowak, D., & Souch, C. (2002). Local-scale fluxes of carbon dioxide in urban environments: Methodological challenges and results from Chicago. *Environmental Pollution*, *116*, S243–S254.

Hoppe, P. (1999). The physiological equivalent temperature −a universal index for the biometeorological assessment. *International Journal of Biometeorology*, *43*, 71–75.

Huttner, S., Bruse, M., & Dostal, P. (2009). Numerical modelling of the urban climate–a preview on ENVI-MET 4.0. *Conf. Urban Clim. 49*.

Innovating to zero the building sector in Europe (2016). Minimizing the energy consumption, eradication of the energy poverty and mitigating the local climate change. *Solar Energy*, *128*(April), 61–94.

Jamei, E., & Ossen, D. R. (2012). Intra urban air temperature distributions in historic urban center. *American Journal of Environmental Science*, *8*, 503–509.

Jihad, A. S., & Tahiri, M. (2016). Modeling the urban geometry influence on outdoor thermal comfort in the case of Moroccan microclimate. *Urban Climate*, *16*, 25–42.

Köppen-Geiger climate classification updated using temperature and precipitation data referring to the period 1951–2000.

Kim, H. H. (1992). Urban heat island. *International Journal of Remote Sensing*, *13*, 2319–2336.

Kolokotroni, M., & Giridharan, R. (2008). Urban heat island intensity in London: An investigation of the impact of physical characteristics on changes in outdoor air temperature during summer. *Solar Energy*, *82*, 986–998.

Kolokotroni, M., Davies, M., Croxford, B., Bhuiyan, S., & Mavrogianni, A. (2010). A validated methodology for the prediction of heating and cooling energy demand for buildings within the Urban Heat Island: Case-study of London. *Solar Energy*, *84*, 2246–2255.

Kong, F., Sun, C., Liu, F., Yin, H., Jiang, F., Pu, Y., et al. (2016). Energy saving potential of fragmented green spaces due to their temperature regulating ecosystem services in the summer. *Applied Energy*, *183*, 1428–1440.

Lauwaet, D., De Ridder, K., Saeed, S., Brisson, E., Chatterjee, F., van Lipzig, N. P. M., et al. (2016). Assessing the current and future urban heat island of Brussels. *Urban Climate*, *15*, 1–15.

Luber, G., & McGeehin, M. (2008). Climate change and extreme heat events. *American Journal of Preventive Medicine*, *35*, 429–435.

Matzarakis, A., Rutz, F., & Mayer, H. (2007). Modelling radiation fluxes in simple and complex environments-application of the RayMan model. *International Journal of Biometeorology*, *51*, 323–334.

McMichael, A. J., Woodruff, R. E., & Hales, S. (2006a). Climate change and human health: Present and future risks. *Lancet*, *367*, 859–869.

McMichael, A. J., Woodruff, R. E., & Hales, S. (2006b). Climate change and human health: Present and future risks. *Lancet*, *367*, 859–869.

Mirzaei, P. A., & Haghighat, F. (2010). Approaches to study urban heat island −Abilities and limitations. *Buildings and Environment*, *45*, 2192–2201.

Mohsin, & Gough, W. A. (2012). Characterization and estimation of urban heat island at Toronto: Impact of the choice of rural sites. *Theoretical and Applied Climatology*, *108*, 105–117.

Morabito, M., Crisci, A., Messeri, A., Orlandini, S., Raschi, A., Maracchi, G., et al. (2016). The impact of built-up surfaces on land surface temperatures in Italian urban areas. *Science of the Total Environment*, *551–552*, 317–326.

Morini, E., Touchaei, A. G., Castellani, B., Rossi, F., & Cotana, F. (2016). The impact of

albedo increase to mitigate the urban heat island in Terni (Italy) using the WRF model. *Sustainability*, *8*(10), 999 [art. no].
Noro, M., Busato, F., & Lazzarin, R. M. (2015). Urban heat island in Padua, Italy : Experimental and theoretical analysis. *Indoor and Built Environment*, *24*, 514–533.
Oke, T. R. (1976). The distinction between canopy and boundary layer urban heat islands. *Atmosphere*, *14*, 268–277.
Papanastasiou, D. K., & Kittas, C. (2012). Maximum urban heat island intensity in a medium/sized coastal Mediterranean city. *Theoretical and Applied Climatology*, *107*, 407–416.
Pisello, A. L., Piselli, C., & Cotana, F. (2015). Thermal-physics and energy performance of an innovative green roof system: The Cool-Green Roof. *Solar Energy*, *116*, 337–356.
Pisello, A. L., Castaldo, V. L., Pignatta, G., Cotana, F., & Santamouris, M. (2016). Experimental in-lab and in-field analysis of waterproof membranes for cool roof application and urban heat island mitigation. *Energy and Buildings*, *114*, 180–190.
Pisello, A. L. (2015). Experimental analysis of cool traditional solar shading systems for residential buildings. *Energies*, *8*(3), 2197–2210.
Rosso, F., Pisello, A. L., Pignatta, G., Castaldo, V. L., Piselli, C., Cotana, F., et al. (2015). Outdoor thermal and visual perception of natural cool materials for roof and urban paving. *Procedia Engineering*, *118*, 1325–1332.
Salata, F., Golasi, I., De Lieto Vollaro, R., & De Lieto Vollaro, A. (2016a). Urban microclimate and outdoor thermal comfort. A proper procedure to fit ENVI-met simulation outputs to experimental data. *Sustainable Cities and Society*, *26*, 318–343.
Salata, F., Golasi, I., de Lieto Vollaro, R., & de Lieto Vollaro, A. (2016b). Outdoor thermal comfort in the Mediterranean area. A transversal study in Rome, Italy. *A Building and Environment*, *96*, 46–61.
Santamouris, M., & Kolokotsa, D. (2015). On the impact of urban overheating and extreme climatic conditions on housing energy comfort and environmental quality of vulnerable population in Europe. *Energy Building*, 98.
Santamouris, M., Cartalis, C., & Synnefa, A. (2015). Local urban warming, possible impacts and a resilience plan to climate change for the historical center of Athens, Greece. *Sustainable Cities and Society*.
Santamouris, M. (2014). On the energy impact of urban heat island and global warming on buildings. *Energy Buildings*, *82*, 100–113.
Stern, N. H., & Treasury, G. B. (2007). *The economics of climate change: The Stern review*. Cambridge Univ Pr.
Stewart, I. D., & Oke, T. R. (2012). Local climate zones for urban temperature studies. *Bams*, 1879–1900.
Taha, H. (1997). Urban climates and heat islands: Albedo, evapotranspiration, and anthropogenic heat. *Energy Buildings*, *25*, 99–103.
Taleghani, M., Kleerekoper, L., Tenpierik, M., & van den Dobbelsteen, A. (2014). Outdoor thermal comfort within five different urban forms in the Netherlands. *Buildings and Environment*, *83*, 65–78.
Terjung, W. H., & O'Rouke, P. A. (1980). Simulating the casual elements of urban heat islands. *Boundary-Layer Meteorology*, *19*, 93–118.
*U.S. department of energy, energy efficiency and renewable energy, energy efficiency and renewable energy*. https://energyplus.net/, https://energyplus.net/weather-location/europe_wmo_region_6/ITA//ITA_Perugia.161810_IGDG, WMO Station Region 6: Italy, Perugia 161810 (IGDG).
Ward, H. C., Kotthaus, S., Grimmond, C. S. B., Bjorkegren, A., Wilkinson, M., Morrison, W. T. J., et al. (2015). Effects of urban density on carbon dioxide exchanges: Observations of dense urban, suburban and woodland areas of southern England. *Environmental Pollution*, *198*, 186–200.
Yang, X., Zhao, L., Bruse, M., & Meng, Q. (2013). Evaluation of a microclimate model for predicting the thermal behavior of different ground surfaces. *Building and Environment*, *60*, 93–104.